Journal of Power Sources 243 (2013) 54–59

Contents lists available at SciVerse ScienceDirect

Journal of Power Sources

journal homepage: www.elsevier.com/locate/jpowsour

Facile synthesis of ultrafine carbon-coated SnO_2 nanoparticles for high-performance reversible lithium storage

Bing Liu, Minhua Cao*, Xinyu Zhao, Yuan Tian, Changwen Hu

Key Laboratory of Cluster Science, Ministry of Education of China, Department of Chemistry, Beijing Institute of Technology, Beijing 100081, PR China

HIGHLIGHTS

- Ultrafine carbon-coated SnO_2 NPs were synthesized by a hydrothermal method.
- Ultrafine carbon-coated SnO_2 NPs have diameters in the ranges of 3–6 nm.
- The NPs exhibit excellent Lithium ion insertion/extraction performance.

ARTICLE INFO

Article history:
Received 26 November 2012
Received in revised form
2 June 2013
Accepted 5 June 2013
Available online 13 June 2013

Keywords:
Tin oxide
Carbon
Anode material
Lithium ion battery

ABSTRACT

Ultrafine carbon-coated SnO_2 nanoparticles (NPs) with diameters of 3–6 nm are prepared by a hydrothermal method in the presence of ascorbic acid and subsequent thermal treatment. The ascorbic acid, on the one hand, serves as a ligand to control the growth of the ultrafine SnO_2 NPs during the hydrothermal process and on the other hand it acts as carbon precursor to form carbon shell surrounding the ultrafine SnO_2 NPs in the thermal treatment process. When evaluated as an anode material for lithium-ion batteries (LIBs), the as-synthesized ultrafine carbon-coated SnO_2 NPs exhibit a high reversible capacity of 688.6 mAh g^{-1} at a rate of 1 C after 50 cycles. Even charging at the rate of as high as 5 C, they still deliver a reversible capacity of 414 mAh g^{-1}, which is about 50% of the theoretical capacity of SnO_2. The perfect electrochemical performance can be ascribed to the synergic effects of the conductive carbon shell surrounding the SnO_2 NPs and the ultra-small size of the SnO_2 NPs.

1. Introduction

The oil shock in 1973 was Europe's first wake-up call. Since then, the increasing consumption of fossil fuel has been driving people to find new alternative energy resources. As one of highly efficient, clean and ideal energies, electrical energy is being received more and more attentions [1–4]. Especially, in the 21st century, the use of portable electronic devices such as laptop computers, mobile phones, digital cameras and electric vehicles is increasing. The portable electronic devices generally require high power density. Lithium-ion batteries (LIBs) are the dominant power source for various types of portable electronic devices because of their high energy density, high voltage, and light weight [2–6]. Carbon-based materials are the most commonly used anode materials during the last century [5–7]. However, the theoretical capacity of graphite (only 372 mAh g^{-1}) is insufficient to satisfy the increasing demand for batteries with higher capacity [7]. Since Fuji Photo Film reported that tin-based oxides exhibited a high capacity, researchers began to focus more on this kind of materials [8,9], in which tin dioxide (SnO_2) received particular attention because it features high theoretical capacity (782 mAh g^{-1}), low cost, and nontoxicity [11]. However, SnO_2 also suffers from large volume change and severe particle aggregation during charge–discharge cycles, which inevitably lead to electrode pulverization and a loss of inter-particle electronic contact and consequently a large irreversible capacity loss and poor cycling stability [10–13].

To date, many efforts have been devoted to solving these problems. An effective strategy is to construct various nanostructures using the bottom-up approach (such as hollow structures, nanospheres, nanosheets, quantum dots, and so on) [4,14–16]. For example, with regard to the hollow structure, the empty spaces could partially accommodate the large volume change during cycling and thus severe capacity fading can be avoided [2,17–19]. Another commonly used alterative strategy is to synthesize carbon-coated nanocomposite materials [5,6,20]. Carbon coating has been addressed to be an effective way for improving the cyclic retention of the oxide-based anode materials for LIBs [20]. In this case, carbon has a dual function. On the one hand, carbon acts as a physical buffering

* Corresponding author. Tel.: +86 10 68918468; fax: +86 10 68918572.
E-mail address: caomh@bit.edu.cn (M. Cao).

0378-7753/$ – see front matter © 2013 Elsevier B.V. All rights reserved.
http://dx.doi.org/10.1016/j.jpowsour.2013.06.017

layer for the large volume change of active materials accompanying Li^+ insertion and extraction in charge/discharge process and on the other hand, it also could effectively increase the electrical conductivity of the electrode materials [5,6,20]. Despite the improvement of electrochemical properties via these strategies, recent studies show that either design strategy alone leads to only limited enhancement in performance [4,7]. Therefore, most researchers generally combine above two strategies in one electrode material in order to obtain perfect electrochemical performance. For example, Lou et al. [21] recently demonstrated the concept by synthesizing coaxial SnO_2@-carbon hollow spheres. This structure incorporates simultaneously two desirable design rationales for high-energy anode materials based on Li-metal alloying, hollow interior space and carbon nanopainting. These coaxial SnO_2@carbon hollow spheres indeed exhibit exceptional cycle life for at least several hundred cycles and good rate capability when evaluated for lithium-storage properties.

Herein, we integrated aforementioned two design strategies and synthesized ultrafine carbon-coated SnO_2 nanoparticles (NPs) with diameters of 3–6 nm using a hydrothermal method in the presence of ascorbic acid and subsequent heat treatment. On the one hand, the ascorbic acid serves as a ligand to control the growth of the ultrafine SnO_2 NPs [22], and on the other hand it acts as carbon precursor for carbon coating. When evaluated as an anode material for LIBs, the ultrafine carbon-coated SnO_2 NPs exhibit a high specific capacity of 688.6 mAh g^{-1} at the rate of 1 C after 50 cycles. Even charging at the rate of as high as 5 C, they still can maintain about 50% of the theoretical capacity of SnO_2. The excellent electrochemical performance of the ultrafine carbon-coated SnO_2 NPs can be attributed to the synergetic effects of the ultrafine particles and carbon-coating.

2. Experimental

2.1. Materials preparation

All chemicals used were analytical grade without further purification. The carbon-coated SnO_2 NPs were synthesized by a simple hydrothermal method followed by a carbonization process. In a typical procedure, 0.2 mmol sodium stannate trihydrate ($Na_2SnO_3 \cdot 3H_2O$) and 0.4 mmol ascorbic acid were added to 60 mL distilled water under stirring at room temperature for 20 min. A clear bright yellow aqueous solution was formed and then the solution was transferred into a 80 mL Teflon-lined stainless steel autoclave. The autoclave was sealed and heated in an air-flow electric oven at 180 °C for 6 h. After being cooled down naturally to room temperature, the obtained brown precipitation was collected by centrifugation and rinsed several times using distilled water and alcohol, and dried in air at room temperature. The as-synthesized sample was further annealed at 500 °C for 2 h in a N_2 flow at a ramp rate of 5 °C min^{-1} to obtain the final product, which then was further characterized. For comparison, the sample obtained in the absence of ascorbic acid was named as SnO_2 NPs.

2.2. Materials characterization

The crystal structure of the as-synthesized products was characterized by X-ray power diffraction (XRD, Shimadzu XRD-6000, Cu-Kα, $\lambda = 1.54178$ Å). The micro-structure and morphology were investigated by field-emission scanning electron microscope (FE-SEM, JEOL S-4800), transmission electron microscope (TEM, JEOL, JEM-2010, 200 kV) and high-resolution transmission electron microscope (HRTEM). The surface area and pore size of SnO_2 NPs were measured using a Belsorp-max surface area detecting instrument by N_2 physisorption at 77 K. The thermogravimetric analysis (TGA) was carried out on a Simultaneous DSC–TG (SDT) Q600 unit in the air atmosphere with a heating rate of 10 °C min^{-1} and FT-IR spectrum was recorded on a Nicolet 170SXFT-IR spectrometer (400–4000 cm^{-1}). UV–vis spectra were taken on a LabTech UV-Power diode array spectrometer with an optical path of 1 cm.

2.3. Electrochemical measurements

To test the electrochemical performance of the carbon-coated SnO_2 NPs, two-electrode CR2025 coin cell (20 d × 2.5 mm) with working electrode and lithium sheet as the reference electrode were assembled in an argon-filled glove-box. The working electrode was prepared by coating slurry onto a Cu foil substrate. The slurry was made by the active material (carbon-coated SnO_2 NPs), conductive carbon black, and polyvinylidene fluoride (PVDF) in the weight ratio of 80:10:10 dissolved in N-methyl pyrrolidone (NMP), in which the mass of the carbon-coated SnO_2 NPs is 1.02 mg. After coating, the electrode was pressed at 10 MPa and dried at 120 °C under vacuum for 48 h. A solution of 1 M $LiPF_6$ in ethylene carbonate (EC)/dimethyl carbonate (DMC)/diethyl carbonate (DEC) (1:1:1 in volume) was used as electrolyte. The cycling performance of the homemade coin cell was measured on a multi-channel battery testing system (LAND CT2001A) in the voltage range of 1.20–0.01 V versus Li/Li^+. Cyclic voltammetry test was recorded on a CHI-660D potentiostat in the potential range of 3.00–0.01 V at a sweep rate of 0.5 mV s^{-1}. The impedance spectra were obtained by applying a sine wave with amplitude of 5 mV over the frequency range from 100 kHz to 0.01 Hz and the electrode potential was 2.4 V.

3. Results and discussion

The preparation of the ultrafine carbon-coated SnO_2 NPs follows two steps. First, ultrafine SnO_2 NPs were formed by the hydrothermal treatment of sodium stannate trihydrate aqueous in the presence of ascorbic acid. Then the ultrafine SnO_2 NPs were annealed under an inert atmosphere and thus a thin carbon layer from carbonization of absorbed organic residues was generated on the surface of the SnO_2 NPs, resulting in the formation of the ultrafine carbon-coated SnO_2 NPs.

The composition of the as-synthesized products was characterized by X-ray diffraction (XRD). Fig. 1 shows the XRD patterns of the as-prepared samples before and after carbonization in N_2 at 500 °C for 2 h, respectively. It can be clearly seen that for the sample obtained directly from hydrothermal process, all identified peaks can be perfectly indexed to the tetragonal rutile structure of SnO_2 (JCPDS card No. 41-1445) and no other crystalline impurities are detected [23], indicating that pure SnO_2 can be obtained under the hydrothermal conditions. The significant broadening and reduced

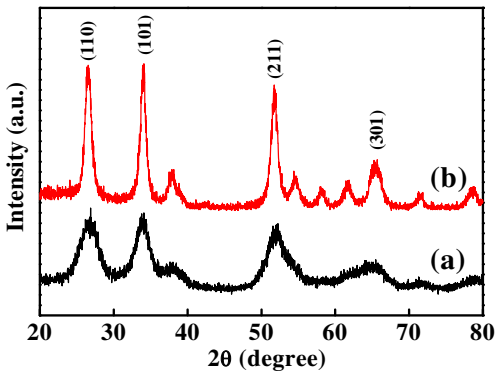

Fig. 1. XRD patterns of (a) the ultrafine SnO_2 NPs obtained directly from hydrothermal process and (b) the ultrafine carbon-coated SnO_2 NPs.

intensity of the diffraction peaks further confirm the ultra-small size of the sample.

To further confirm the existence of organic residues on the surface of the ultrafine SnO_2 NPs, Fourier transform infrared (FT-IR) spectra were carried out, as shown in Fig. 2a. The absorption peaks at about 3408 and 1668 cm^{-1} could be ascribed to the O–H vibration of the absorbed water in the sample. The bands at 1079 cm^{-1} and 952 cm^{-1} are both identified as surface hydroxyl groups [24–26]. The absorption peaks at 2948 and 1380 cm^{-1} are attributed to the C–H stretching vibration, which should result from the decomposition products of the used ascorbic acid, indicating the existence of organic compounds in the ultrafine SnO_2 NPs [24–26]. Therefore, we deduce that the ascorbic acid used in our experiment is decomposed into other organic compounds during the hydrothermal process, which then adsorb on the surface of the formed SnO_2 particles to prevent them from overgrowth and agglomeration. At the same time, the adsorbed decomposition products may serve as carbon precursor to form carbon coating in subsequent annealing process. On the other hand, the ascorbic acid can decrease the growth rate of SnO_2 crystals, ensuring the formation of the ultrafine SnO_2 NPs since the ascorbic acid and Na_2SnO_3 could form a complex in the solution after mixturing. As shown in Fig. 2b, the mixed aqueous solution of the ascorbic acid and Na_2SnO_3 exhibits a yellow color, indicating the formation of Sn–ascorbic acid coordination compound. This phenomenon can be further confirmed by ultraviolet–visible (UV–vis) spectra (Fig. 2c). After calcining at 500 °C for 2 h in a N_2 flow, ultra-fine carbon-coated SnO_2 NPs were formed. As shown in Fig. 1b, all diffraction peaks become much narrower in width and stronger in intensity compared to those of the sample before carbonization, suggesting slightly enlarging of SnO_2 NPs during the heat treatment process.

To determine the carbon content in the as-synthesized carbon-coated SnO_2 NPs, thermogravimetric analysis (TGA) was carried out from room temperature to 600 °C at a ramp rate of 10 °C min^{-1} in air. As shown in Fig. 2d, the first slight weight loss of about 1.5% between 50 and 100 °C, corresponds to the removal of water weakly absorbed on the surface of the carbon-coated SnO_2 NPs. The second weight loss of 14.5% occurring between 100 and 500 °C, can be ascribed to the elimination of oxygen combustion of organic carbon existed in carbon-coated SnO_2 NPs. It is expected that the carbon layer on the surface of SnO_2 NPs can buffer severe volume change during Li^+ insertion/extraction and improve the conductivity of the SnO_2 NPs.

The morphology and microstructure of the carbon-coated SnO_2 sample are investigated with transmission electron microscopy (TEM). Fig. 3a–c shows TEM images of the carbon-coated SnO_2 sample at different magnifications, which clearly reveal that the sample consists entirely of relatively uniform NPs. The size of the NPs is around 3–6 nm in diameter. The selected area electron diffraction (SAED) (Fig. 3d) pattern appears as individual spots associated with concentric rings, indicating the polycrystalline nature of the carbon-coated SnO_2 NPs. Fig. 3e shows a high resolution TEM (HRTEM) image of the same sample, from which it can be seen that each particle exhibits very clear crystal lattice, disclosing high crystallinity of the ultrafine NPs. Furthermore, amorphous carbon layer with a thickness of a few nanometers can also be clearly observed between the NPs (Fig. 3f) (marked by arrows). The presence of carbon as well as its content has been confirmed by above TGA in air. For comparison, we also carried out the experiment in the absence of ascorbic acid while keeping all other conditions the same. The as-obtained sample is also SnO_2 phase, but it exhibits a spherical nanostructure with a larger size, which has been confirmed by XRD pattern and SEM (Fig. 4a). This result provides the fact that ascorbic acid plays an important role in the formation of the ultrafine carbon-coated SnO_2 NPs.

As expected, nitrogen adsorption/desorption measurement shows that the ultrafine carbon-coated SnO_2 NPs possess a high Brunauer–Emmett–Teller (BET) specific surface area of *ca.* 118.21 $m^2\ g^{-1}$, which is far larger than that of the sample obtained

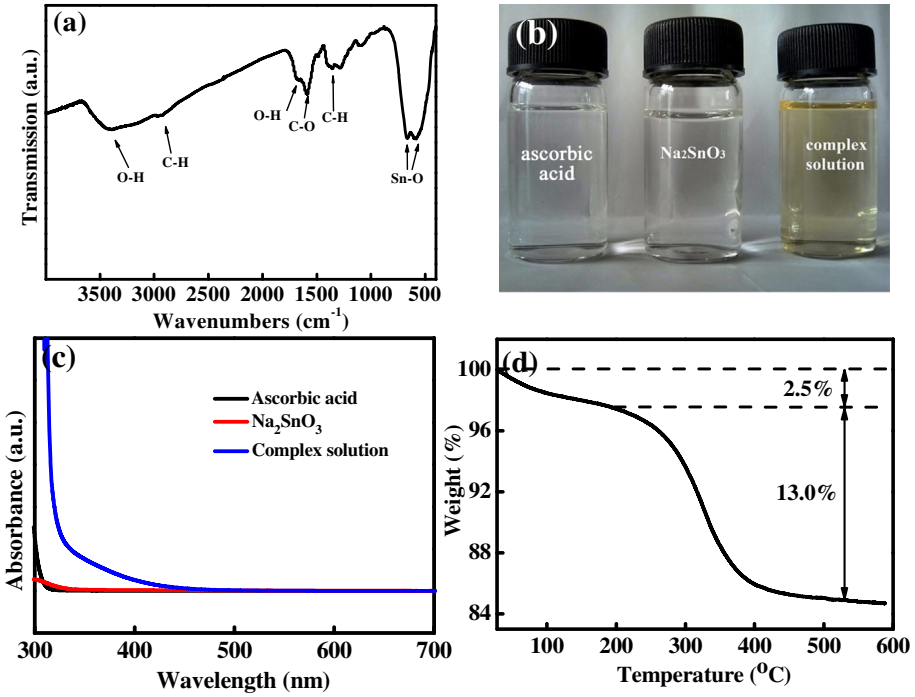

Fig. 2. (a) FT-IR spectrum of the ultrafine carbon-coated SnO_2 NPs. (b) The photographs, (c) UV–vis spectra of the aqueous solutions of two starting materials (Na_2SnO_3 and ascorbic acid) and corresponding complex. (d) TGA of the ultrafine carbon-coated SnO_2 NPs.

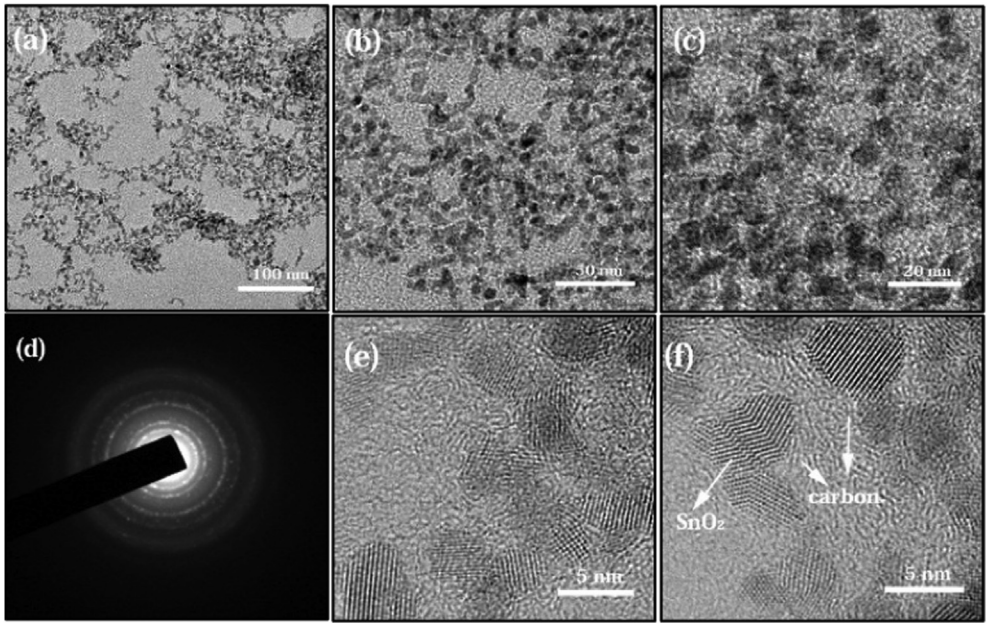

Fig. 3. (a–c) TEM images with different magnifications, (d) SAED and (e,f) high-resolution TEM images of the as-prepared ultrafine carbon-coated SnO_2 NPs.

without ascorbic acid. As shown in Fig. 4b, the N_2 adsorption–desorption isotherm is of type IV with a hysteresis at the relative pressure of 0.4–0.8 and has a large N_2 uptake at low relative pressures, indicating that the ultrafine SnO_2 NPs possess a microporous/mesoporous hierarchical structure. We deduce that the high specific surface area and the hierarchical structure mainly result from the porous carbon layer. This distinct structure and high specific surface area may provide a large number of active sites for charge-transfer reactions, and therefore the ultrafine carbon-coated SnO_2 NPs are expected to exhibit enhanced Li storage capacity and improved rate capability.

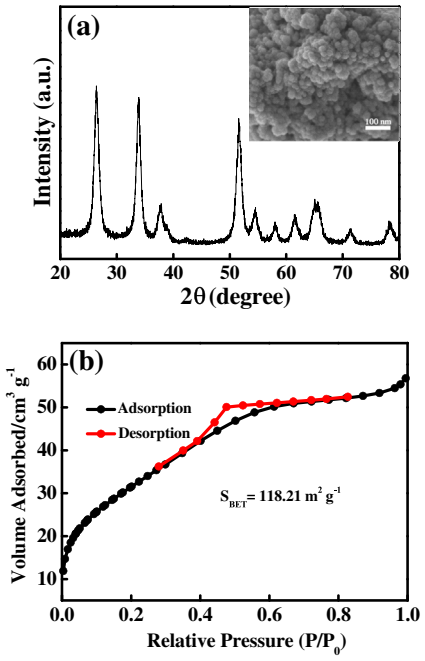

Fig. 4. (a) XRD pattern of SnO_2 NPs obtained without ascorbic acid, and inset is SEM image. (b) Nitrogen adsorption/desorption isotherms of the as-prepared ultrafine carbon-coated SnO_2 NPs.

The potential use of the ultrafine carbon-coated SnO_2 NPs as an anode material for LIBs is then investigated and results show that the ultrafine carbon-coated SnO_2 NPs exhibit greatly improved electrochemical performance compared to nanostructured counterpart. First, to better understand the electrode reaction process of the ultrafine carbon-coated SnO_2 NPs, cyclic voltammetric measurements (CV) were carried out. As shown in Fig. 5a, the CV behavior is in well agreement with those reported in previous papers [5], indicating the same reaction mechanism. In the first cycle an apparent reduction peak at around 0.72 V (versus Li/Li^+) is observed, which can be ascribed to the formation of solid electrolyte interphase (SEI), the reduction of SnO_2 to Sn, and the formation of Li_2O when SnO_2 phase reacts with Li^+ ($SnO_2 + 4Li^+ + 4e^- \rightarrow Sn + 2Li_2O$). This peak disappears after the first cycle, leaving a large initial irreversible capacity, while in the following cycles, a new peak at about 0.86 V appears, suggesting the fact that the irreversible reaction was still taking place until the filth cycle. Another reduction peak around at 0.10 V is attributed to the formation of Li*x*Sn alloy ($Sn + xLi^+ + xe^- \leftrightarrow$ Li*x*Sn). Furthermore, two oxidation peaks are also observed. The one at 0.6 V corresponds to the dealloying process of the Li_xSn alloy and the other at 1.30 V might indicate the partial reversibility of the reaction ($SnO_2 + 4Li^+ + 4e^- \rightarrow Sn + 2Li_2O$). Fig. 5b shows the representative discharge and charge curves of the ultrafine carbon-coated SnO_2 nanoparticle electrode from the first to the fiftieth cycle at a high rate of 1 C (where 1 C = 782 mA g^{-1}) in the potential range of 1.20–0.01 V. The initial discharge and charge capacities are 709.8 and 1830.6 mAh g^{-1}, respectively. The initial capacity loss can be ascribed to the irreversible lithium loss during the first cycle due to the formation of SEI film and electrolyte decomposition, which are common for most anode materials [4]. Although the irreversible capacity ratio, in our case, is as high as 61%, the reversible capacity after 5 cycles can still stabilize at around 700 mAh g^{-1} at a high rate of 1 C, which is higher than those of most reported SnO_2 tested under same conditions [2]. And also this reversible capacity could keep almost constant until the fiftieth cycle. In contrast, for the sample (SnO_2 NPs) obtained in the absence of ascorbic acid, its reversible capacity drops to 155 mAh g^{-1} after the fiftieth cycle (Fig. 5c,d). The Coulombic efficiency of the ultrafine carbon-coated SnO_2 NPs rises rapidly from 39% in the first cycle to

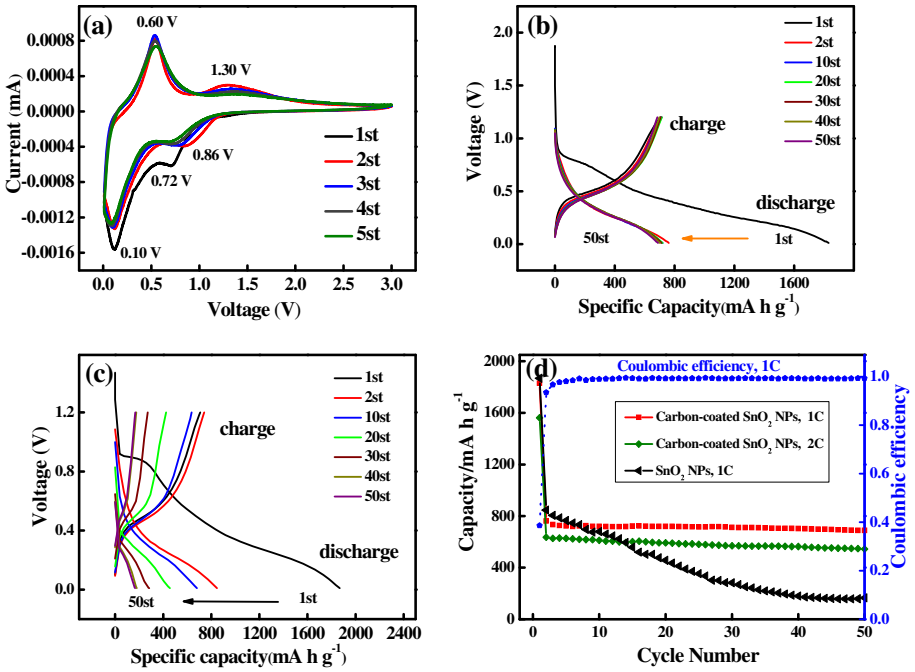

Fig. 5. (a) The cyclic voltammetry of the ultrafine carbon-coated SnO_2 NPs at a rate of 0.5 mV s^{-1}. (b,c) The discharge/charge voltage profiles of the ultrafine carbon-coated SnO_2 NPs and the SnO_2 NPs at 1 C rate. (d) Cycling performance of the ultrafine carbon-coated SnO_2 NPs and SnO_2 NPs.

98% in the fifth one and then remains above 99% in the following cycles (Fig. 5d). The discharge–charge cycling performance is also evaluated at 1 C up to 50 cycles, as shown in Fig. 5d. It can be clearly seen that it displays exceptional cyclability compared to other SnO_2-based anode materials at same rate. Specifically, while the capacity decays gradually over the first 5 cycles, it rapidly stabilizes around 700 mAh g^{-1} for more than 50 cycles. When the rate is increased to 2 C, it still can deliver a very stable capacity of about 541.6 mAh g^{-1}.

In addition, another amazing enhancement for the ultrafine carbon-coated SnO_2 sample is its remarkable rate capability. As shown in Fig. 6a, the ultrafine carbon-coated SnO_2 electrode is observed to show high specific capacity at all tested rates. For example, at a high rate of 5 C, the cell can still deliver a high capacity of around 400 mAh g^{-1}, which is close to 50% of the theoretical capacity of SnO_2. That means it will take a little time to complete a charge or discharge process. In addition, it should be noted that when the current rate is reduced back to 1 C again, a capacity of higher than 600 mAh g^{-1} can be resumed. The perfect electrochemical performance may result from the ultrafine size and carbon content of the carbon-coated SnO_2 NPs.

To further understand the evidently improved rate and exceptional cyclability performance, electrochemical impedance spectroscopy (EIS) measurements on the ultrafine carbon-coated SnO_2 NPs and SnO_2 NPs were performed from 100 kHz to 0.01 Hz before charge–discharge test. As shown in Fig. 6b, both Nyquist plots consist of one depressed semicircle at high frequencies and a straight line at low frequencies, but the diameter of the semicircle of the carbon-coated SnO_2 NPs electrode in the high frequency region is much smaller than that of the electrode made of SnO_2 NPs [27,28]. Thus, the ultrafine carbon-coated SnO_2 NPs have lower contact and charge-transfer impedances when used as electrode materials, i.e. improved conductivity. As a consequence, Li ions diffusion and electron transfer are expedited at high cycling rates. Therefore, the improved rate performance may be attributed to the increased conductivity of the ultrafine carbon-coated SnO_2 NPs.

Considering that both samples are composed of SnO_2 NPs, the evidently enhanced specific capacity, higher rate capability, and exceptional cycling stability of the ultrafine carbon-coated SnO_2 NPs can be ascribed to the following factors according to above studies. On one hand, the carbon shell surrounding the ultrafine

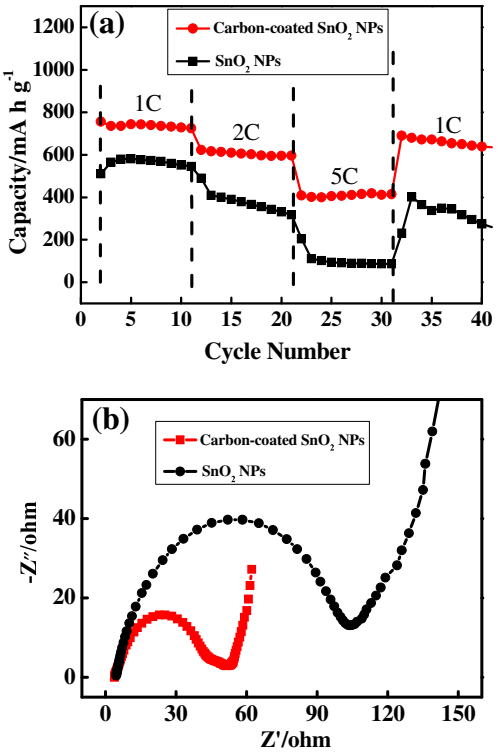

Fig. 6. (a) The rate performance and (b) electrochemical impedance spectroscopies of the ultrafine carbon-coated SnO_2 NPs and SnO_2 NPs.

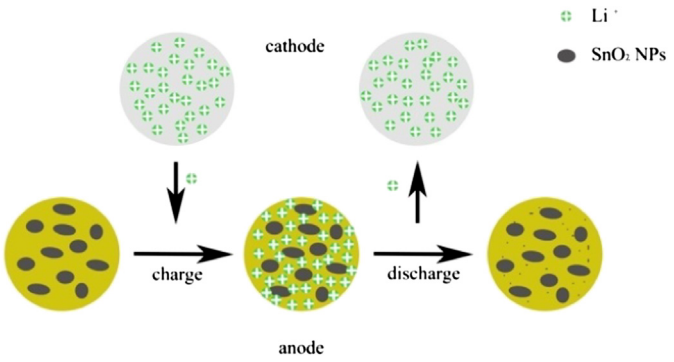

Scheme 1. Schematics of the insertion/extraction process of lithium ions into the ultrafine carbon-coated SnO_2 NPs.

SnO_2 NPs not only acts as a buffer layer that could efficiently alleviate the volume change during the insertion/extraction of lithium ions in the charge/discharge process, but also can increase the conductivity of the active materials. On the other hand, the ultrasmall size of the SnO_2 NPs leads to the bigger specific surface area, which could provide much more spaces to accommodate lithium ions during lithium insertion/extraction process and at the same time it is also helpful for buffering the severe volume change. Therefore, this strategy combining carbon coating and ultrafine particles is an effective way to improve the electrochemical performance of SnO_2 for LIBs.

Scheme 1 simply shows the schematics of the insertion/extraction of the lithium ions into the ultrafine carbon-coated SnO_2 NPs. During charging, Li^+ transfers from the cathode to anode electrode through the non-aqueous electrolyte and separator. Due to enough space and carbon shell around the SnO_2 particles, the SnO_2 will hold more inserted Li^+ and at the same time the SnO_2 NPs will keep original shape after discharging. These features will be beneficial for the long cycle life and cycling stability of the as-synthesized SnO_2 NPs, which is agreement with well the result of Refs. [2,29–31].

4. Conclusion

In conclusion, we have demonstrated the synthesis of the ultrafine carbon-coated SnO_2 NPs in the presence of ascorbic acid via a hydrothermal method and subsequent heat treatment. The ultrafine carbon-coated SnO_2 NPs have sizes in the range of 3–6 nm. The ascorbic acid used in our case serves as a ligand to control the growth of the ultrafine SnO_2 NPs during the hydrothermal process and on the other hand it acts as a carbon precursor for carbon shell. When the ultrafine carbon-coated SnO_2 NPs were applied as an anode material for LIBs, they exhibited high specific capacity and excellent rate performance. The result demonstrates that the strategy combing ultrafine NPs and carbon-coating is an effective way to improve the electrochemical performance of the oxide-based anode materials in LIBs. In addition, our simple, straightforward strategy can be further extended to prepare other nanomaterials.

Acknowledgments

This work was supported by the Natural Science Foundation of China (NSFC, Nos. 21231002, 21276026, 21271023, 21173021, 91022006 and 20973023), the 111 Project (B07012), Program for New Century Excellent Talents in University, Specialized Research Fund for the Doctoral Program of Higher Education (SRFDP, No. 20101101110031).

References

[1] M. Armand, J.M. Tarascon, Nature 451 (2008) 652.
[2] J.S. Chen, L.A. Archer, X.W. Lou, J. Mater. Chem. 21 (2011) 9912.
[3] M.S. Park, G.X. Wang, Y.M. Kang, D. Wexler, S.X. Dou, H.K. Liu, Angew. Chem. Int. Ed. 46 (2007) 750.
[4] X.W. Lou, Y. Wang, C. Yuan, J.Y. Lee, L.A. Archer, Adv. Mater. 18 (2006) 2325.
[5] R. Yang, W. Zhao, J. Zheng, X.Z. Zhang, X.G. Li, J. Phys. Chem. C 114 (2010) 20272.
[6] Y.S. Lin, J.G. Duh, M.H. Hung, J. Phys. Chem. C 114 (2010) 13136.
[7] X.W. Lou, D. Deng, J.Y. Lee, L.A. Archer, Chem. Mater. 20 (2008) 6562.
[8] H. Wang, Y.M. Wu, Y.S. Bai, W. Zhou, Y.R. An, J.H. Li, L. Guo, J. Mater. Chem. 21 (2011) 10189.
[9] Z.P. Guo, G.D. Du, Y. Nuli, M.F. Hassan, H.K. Liu, J. Mater. Chem. 19 (2009) 3253.
[10] X.M. Yin, C.C. Li, M. Zhang, Q.Y. Hao, S. Liu, L.B. Chen, T.H. Wang, J. Phys. Chem. C 114 (2010) 8084.
[11] J.X. Li, Y. Zhao, N. Wang, L.H. Guan, Chem. Commun. 47 (2011) 5238.
[12] Y.M. Li, X.J. Lv, J. Lu, J.H. Li, J. Phys. Chem. C 114 (2010) 21770.
[13] M. Noh, Y. Kwon, H. Lee, J. Cho, Y. Kim, M.G. Kim, Chem. Mater. 17 (2005) 1926.
[14] D. Deng, J.Y. Lee, Chem. Mater. 20 (2008) 1841.
[15] G.C. Xi, J.H. Ye, Inorg. Chem. 49 (2010) 3553.
[16] L.Y. Jiang, X.L. Wu, Y.G. Guo, L.J. Wan, J. Phys. Chem. C 113 (2009) 14213.
[17] S.J. Ding, J.S. Chen, G.G. Qi, X.N. Duan, Z.Y. Wang, E.P. Giannelis, L.A. Archer, X.W. Lou, J. Am. Chem. Soc. 133 (2011) 21.
[18] Z.Y. Wang, D.Y. Luan, C.B. Frddly Yin, X.W. Lou, J. Am. Chem. Soc. 133 (2011) 4738.
[19] C. Wang, G.H. Du, K. Stahl, H.X. Huang, Y.J. Zhong, J.Z. Jiang, J. Phys. Chem. C 116 (2012) 4000.
[20] G.L. Xu, S.R. Chen, J.T. Li, F.S. Ke, L. Huang, S.G. Sun, J. Electroanal. Chem. 656 (2011) 185.
[21] X.W. Lou, C.M. Li, L.A. Archer, Adv. Mater. 21 (2009) 2536.
[22] L.Y. Feng, M.H. Cao, X.Y. Ma, Y.S. Zhu, C.W. Hu, J. Hazard. Mater. 217–218 (2012) 439.
[23] S.J. Ding, X.W. Lou, Nanoscale 3 (2011) 3586.
[24] H.J. Wang, F.Q. Sun, Y. Zhang, L.S. Li, H.Y. Chen, Q.S. Wu, J.C. Yu, J. Mater. Chem. 20 (2012) 5641.
[25] D. Solis-Casados, E. Vigueras-Santiago, S. Hernandez-Lopez, M.A. Camacho-Lopez, Ind. Eng. Chem. Res. 48 (2009) 1249.
[26] S.H. Wu, H.Q. Cao, S.F. Yin, X.W. Liu, X.R. Zhang, J. Phys. Chem. C 113 (2009) 17893.
[27] P. Wu, N. Du, H. Zhang, C.N. Zhai, D.R. Yang, ACS Appl. Mater. Interf. 3 (2011) 1946.
[28] X.Y. Zhao, M.H. Cao, B. Liu, Y. Tian, C.W. Hu, J. Mater. Chem. 22 (2012) 13334.
[29] F.Y. Cheng, J. Liang, Z.L. Tao, J. Chen, Adv. Mater. 23 (2011) 1695.
[30] M.S. Whittingham, Chem. Rev. 104 (2004) 4271.
[31] Z.G. Yang, J.L. Zhang, M.W.K. Meyer, X.C. Lu, D. Choi, J.P. Lemmon, J. Liu, Chem. Rev. 111 (2011) 3577.